Applied Catalysis B: Environmental 152–153 (2014) 317–327

Contents lists available at ScienceDirect

Applied Catalysis B: Environmental

journal homepage: www.elsevier.com/locate/apcatb

Catalytic conversion of 1,2-dichloroethane over bimetallic Cu–Ni loaded BEA zeolites

Anna Śrębowata[a,**], Rafal Baran[b,c,d], Sandra Casale[c], Izabela I. Kamińska[a], Dariusz Łomot[a], Dmytro Lisovytskiy[a], Stanislaw Dzwigaj[c,d,*]

[a] Institute of Physical Chemistry, PAS, ul. Kasprzaka 44/52, PL-01224 Warszawa, Poland
[b] AGH University of Science and Technology, al. A. Mickiewicza 30, 30-059 Krakow, Poland
[c] Sorbonne Universités, UPMC Univ Paris 06, UMR 7197, Laboratoire de Réactivité de Surface, F-75005, Paris, France
[d] CNRS, UMR 7197, Laboratoire de Réactivité de Surface, F-75005, Paris, France

ARTICLE INFO

Article history:
Received 12 October 2013
Received in revised form 21 January 2014
Accepted 27 January 2014
Available online 2 February 2014

Keywords:
Cu–Ni
Beta zeolites
1,2-dichloroethane
Hydrodechlorination
Dehydrochlorination

ABSTRACT

Beta zeolites with two different Si/Al ratios of 17 and 1500 were used for synthesis Cu_xNi_yHAlBEA and Cu_xNi_ySiBEA zeolites by conventional wet impregnation and two-step postsynthesis procedure, respectively. The calcination of Cu_xNi_yHAlBEA and Cu_xNi_ySiBEA at 773 K for 3 h in air led to the formation of C-Cu_xNi_yHAlBEA and C-Cu_xNi_ySiBEA with appearance, for the latter mainly pseudo-tetrahedral Ni(II) and Cu(II) incorporated in BEA framework and for the former, both framework pseudo-tetrahedral and extra-framework octahedral Ni(II) and Cu(II) species as evidenced by XRD, DR UV–vis and XPS. Bimetallic red-C-Cu_xNi_yHAlBEA and red-C-Cu_xNi_ySiBEA catalysts obtained by treatment of C-Cu_xNi_yHAlBEA and C-Cu_xNi_ySiBEA at 873 K for 3 h in flowing 10% H_2/Ar stream were investigated in gas phase conversion of 1,2-dichloroethane at atmospheric pressure towards desired products (vinyl chloride and ethylene), at relatively low reaction temperature (523 K). Red-C-Cu_xNi_yHAlBEA catalysts were active in dehydrochlorination of 1,2-dichloroethane with ~100% of selectivity to vinyl chloride. In contrast, for red-C-Cu_xNi_ySiBEA, ~100% of selectivity to ethylene were obtained by hydrodechlorination of 1,2-dichloroethane. Behaviour of both kinds of catalysts in catalytic conversion of 1,2-dichloroethane depends mainly on the nature of bimetallic Ni–Cu nanoparticles, their dispersion and the acidity of zeolite supports.

1. Introduction

Chlorinated hydrocarbons are widely used in chemical industry as solvents, extractants, dry-cleaners, degreasing agents and specially adhesives. However released into the environment are hazardous contaminants [1].

Reaction involving hydrogen in the presence of catalyst is one of the most efficient method for transformation of chloroorganic compounds (COCs) to non-toxic, environmentally friendly products or industrially useful substances [2]. Particular attention as promising catalysts in this kind of reactions play bimetallic materials composed with noble (Pd, Pt) and another transition metals (Fe, Cu, Ni, Ag) supported on oxides like Al_2O_3, SiO_2 or active carbons [3–8] because monometallic catalysts deactivate faster due to coke formation and metal sintering as well as selectivity toward unsaturated hydrocarbons, industrially more valuable products, is much lower when only noble metals are applied [3–8].

Moreover, because of high market price of precious element new materials prepared with less expensive compounds are searched. Recently, in some reactions the bimetallic Cu–Ni materials were tested as catalysts [9–12]. They were applied for the synthesis of dimethyl carbonate [9], partial oxidation of methane [10], ethanol reforming [11] or in hydrogenation of citral [12]. It has been earlier reported that addition of copper to the nickel catalysts enhances the selectivity to unsaturated hydrocarbons, the most desired products of transformation of chloroorganic compounds [13].

It was shown [14–16] that a very important role in conversion of chloroorganic compounds could play the support. It was reported that the use of materials with acidic sites strongly influenced both activity and selectivity of the catalysts [14,15]. In particular,

* Corresponding author at: Université Pierre et Marie Curie, Laboratoire de Réactivité de Surface, UMR 7609-CNRS 4 place Jussieu, Tour 54-55, 75252 >2ème étage, Paris, France. Tel.: +33 1 44 27 21 13; fax: +33 1 2203405057.
** Corresponding author at: Institute of Physical Chemistry, PAS, ul. Kasprzaka 44/52, PL-01224 Warszawa, Poland. Tel.: +48 22 343 3215.
E-mail addresses: asrebowata@ichf.edu.pl (A. Śrębowata), stanislaw.dzwigaj@upmc.fr (S. Dzwigaj).

0926-3373/$ – see front matter © 2014 Elsevier B.V. All rights reserved.
http://dx.doi.org/10.1016/j.apcatb.2014.01.052

the presence in catalysts of strong Brønsted acidic sites led to the formation of products of dehydrochlorination of chloroorganic compounds [15,16].

In this work, the effect of the preparation procedure, a conventional wet impregnation and a two-step postsynthesis method on the nature of active centers formed in bimetallic red-C-Cu_xNi_yHAlBEA and red-C-Cu_xNi_ySiBEA catalysts and their catalytic activity in conversion of 1,2-dichloroethane were investigated. The catalysts before and after reaction were characterized by chemical analysis, X-ray diffraction (XRD), temperature-programmed reduction (TPR), diffuse reflectance UV–vis spectroscopy (DR UV–vis), X-ray photoelectron spectroscopy (XPS), low temperature N_2 sorption, transmission electron microscopy (TEM) to investigate the type of Cu–Ni species occurring in BEA zeolite upon different steps of preparation of the catalysts. To detect the species that can be removed from spent catalysts by treatment with hydrogen a temperature-programmed hydrogenation (TPH) was used.

2. Experimental

2.1. Catalysts preparation

A tetraethylammonium BEA (TEABEA) (Si/Al = 17) zeolite provided by RIPP (China) was calcined for 15 h at 823 K to remove template. Organic-free BEA zeolite was separated into two portions. The first portion was treated with 13 mol L^{-1} nitric acid (353 K, 4 h) to obtain dealuminated SiBEA zeolite and then washed several times with distilled water and dried at 363 K overnight. Results of chemical analysis indicate that only traces of Al remain in SiBEA after nitric acid treatment with Si/Al ratio of 1500.

Second fraction of calcined BEA zeolite was treated two times with 0.1 mol L^{-1} NH_4NO_3 solution during 3 h. Then, the solid was washed with distilled water and dried overnight at 363 K. The resulted NH_4AlBEA was calcined in air at 773 K for 3 h to remove NH_3 and obtain acidic form of zeolite BEA, HAlBEA (Si/Al = 19).

Cu_xNi_ySiBEA and Cu_xNi_yHAlBEA (x = 2 or 4 Cu wt.% and y = 2 Ni wt.%) were prepared by co-impregnation of 2 g of SiBEA and HAlBEA with $Ni(NO_3)_2{\cdot}6H_2O$ and $Cu(NO_3)_2{\cdot}6H_2O$ solutions with appropriate concentration of Cu and Ni, respectively. Firstly, all suspensions were stirred for 24 h at 298 K in excess solvent using 200 mL of the precursor solutions. Then, the suspensions were stirred for 2 h in air at 333 K until complete evaporation of water. The catalysts obtained in this ways are labeled $Cu_{2.0}$SiBEA, $Cu_{2.0}Ni_{2.0}$SiBEA, $Cu_{4.0}Ni_{2.0}$SiBEA, $Cu_{2.0}$HAlBEA, $Cu_{2.0}Ni_{2.0}$HAlBEA and $Cu_{4.0}Ni_{2.0}$HAlBEA. All these materials were calcined in static air at 773 K for 3 h and labeled C-$Cu_{2.0}$SiBEA, C-$Cu_{2.0}Ni_{2.0}$SiBEA, C-$Cu_{4.0}Ni_{2.0}$SiBEA, C-$Cu_{2.0}$HAlBEA, C-$Cu_{2.0}Ni_{2.0}$HAlBEA and C-$Cu_{4.0}Ni_{2.0}$HAlBEA, respectively. Then, a portion of these materials were reduced at 873 K, for 3 h in flowing 10% H_2/Ar to obtain red-C-$Cu_{2.0}$SiBEA, red-C-$Cu_{2.0}Ni_{2.0}$SiBEA, red-C-$Cu_{4.0}Ni_{2.0}$SiBEA, red-C-$Cu_{2.0}$HAlBEA, red-C-$Cu_{2.0}Ni_{2.0}$HAlBEA and red-C-$Cu_{4.0}Ni_{2.0}$HAlBEA where C stands for calcined and red for reduced. These catalysts after kinetic run were labeled with additional prefix spent- e.g. as spent-red-C-Cu_xNi_ySiBEA.

2.2. Catalyst characterization

Chemical analysis was performed at room temperature on SPECTRO X-Lab Pro apparatus.

X-ray diffractograms (XRD) were recorded at room temperature on a PANalytical Empyrean diffractometer using the CuK_α radiation (λ = 154.05 pm).

DR UV–vis spectra were recorded at ambient atmosphere on a Cary 5000 Varian spectrometer equipped with a double integrator with polytetrafluoroethylene as reference.

X-ray photoelectron spectroscopy (XPS) measurements were performed with a hemispherical analyzer (PHOIBOS 100, SPECS Gmbh) using MgK_α (1253.6 eV) radiation. The power of the X-ray source was 300 W. The area of the sample analysed was ~3 mm^2. The powder samples were pressed on an indium foil and mounted on a special holder. Binding energy (BE) for Si and Ni was measured by reference to the O 1s peak at 532.5 eV, corresponding to the binding energy of oxygen bonded to silicon. Before analysis, zeolite samples were outgassed at room temperature to a pressure of 10^{-7} Pa. All spectra were fitted with a Voigt function (a 70/30 composition of Gaussian and Lorentzian functions) in order to determine the number of components under each XPS peak.

Temperature-programmed reduction (TPR) for all of the catalysts, after calcination step, were carried out using the glass-flow system. TPR runs were performed in flowing 10% H_2/Ar (25 cm^3 min^{-1}), ramping the temperature at 10 K min^{-1} and using a Gow-Mac thermal conductivity detector (TCD). Injections of known amounts of hydrogen into the hydrogen–argon flow were provided for calibration (before and after each TPR run).

TEM studies for the catalysts after reduction step and after catalytic reaction were carried out using JEOL JEM-100CXII electron microscope operated at an acceleration voltage of 100 keV. The samples were prepared by their dispersing in pure alcohol using ultrasonic cleaner and putting a drop of this suspension on carbon films on copper grids. For chosen bimetallic samples the high resolution transmission electron microscopy (HRTEM) and scanning transmission electron microscopy (STEM) in high-angle annular dark-field mode were performed on TAN Cubed electron microscope at 300 kV. Before each HRTEM and STEM measurement catalysts after reduction and after kinetic runs were prepared by mechanical grinding, dispersing in pure alcohol using an ultrasonic generator, putting a drop of this suspension on a copper mesh covered with carbon film and purified with plasma cleaner.

Specific surface area and adsorption isotherms of nitrogen at 77 K were measured on a Micromeretics ASAP 2010 apparatus. All samples were outgassed, first at room temperature, then at 623 K to a pressure <0.2 Pa. The specific surface areas were determined from nitrogen adsorption values from P/P^0 = 0.05 to 0.16 using BET method. The microporous pore volume was determined from the amount of N_2 adsorbed up to P/P^0 = 0.2.

Temperature-programmed hydrogenation (TPH) were carried out by mass spectrometry (MA200, Dycor-Ametek, Pittsburgh) to detect a compound that can be removed by hydrogen from spent catalysts. During the experiments samples after conversion of 1,2-dichloroethane were heated from room to 1073 K in the flow of 20% H_2/He with monitoring of twelve masses (m/z).

2.3. Catalysts activity measurements

Catalytic conversion of 1,2-dichloroethane (1,2-DCE, HPLC grade, 99.8% pure from Sigma–Aldrich, Germany) were carried out at atmospheric pressure, in a glass flow reactor equipped with fritted disk to place a catalyst charge. Prior to reaction, 0.2 g of the catalyst, after calcination step at 773 K, was reduced in flowing 10% H_2/Ar (25 cm^3 min^{-1}), ramping the temperature from room temperature to 873 K (10 K min^{-1}) and kept at 873 K for 3 h. After this time, the catalysts were cooled to 523 K, then contacted with the flowing reaction mixture (H_2 + Ar + 1,2-DCE) of 2.86×10^{-5} mol s^{-1} (42 cm^3 min^{-1}) The contact time was of 0.7 s and the space velocity (SV) of 0.0035 (m^3 kg^{-1} s^{-1}). 1,2-DCE was provided from a saturator kept at 273 K to give the partial pressure of 1,2-dichloroethane of 2.9 kPa. The partial pressure ratio pH_2/p1,2-DCE was 1:1. The flows of H_2 and Ar, were fixed by using Bronkhorst Hi-Tec mass flow controllers. The reaction was followed by gas chromatography, using a HP5890 series II gas chromatograph with FID, a 5% Fluorcol/Carbopack B column (10 ft) from Supelco. The results of

Table 1
Textural properties of SiBEA, $Cu_{2.0}$SiBEA, $Cu_{2.0}Ni_{2.0}$SiBEA, $Cu_{4.0}Ni_{2.0}$SiBEA, HAlBEA, $Cu_{2.0}$HAlBEA, $Cu_{2.0}Ni_{2.0}$HAlBEA and $Cu_{4.0}Ni_{2.0}$HAlBEA.

Samples	Specific surface area S_{BET} ($m^2\ g^{-1}$)	Micropores volume V_{mic} ($cm^3\ g^{-1}$)
SiBEA	577	0.23
$Cu_{2.0}$SiBEA	483	0.19
$Cu_{2.0}Ni_{2.0}$SiBEA	523	0.21
$Cu_{4.0}Ni_{2.0}$SiBEA	390	0.16
HAlBEA	608	0.23
$Cu_{2.0}$HAlBEA	675	0.27
$Cu_{2.0}Ni_{2.0}$HAlBEA	683	0.27
$Cu_{4.0}Ni_{2.0}$HAlBEA	612	0.24

GC analysis were elaborated using HP Chemstation. The total FID signal from the first two analyses was similar to that observed in subsequent GC analyses.

3. Results and discussion

3.1. Textural properties of Cu_xNi_ySiBEA and Cu_xNi_yHAlBEA

The nitrogen adsorption–desorption isotherms of Cu_xNi_ySiBEA and Cu_xNi_yHAlBEA (results not shown) may be classified as type I according to IUPAC. All zeolite materials have similar BET surface area and micropore volume (Table 1) indicating that textural properties of BEA zeolite are preserved upon both methods of their preparation. Only $Cu_{4.0}Ni_{2.0}$SiBEA has lower specific surface area, probably due to the formation of copper and/or nickel oxide which may block access to some pores.

XRD patterns of SiBEA, $Cu_{2.0}$SiBEA, $Cu_{2.0}Ni_{2.0}$SiBEA, $Cu_{4.0}Ni_{2.0}$SiBEA and HAlBEA, $Cu_{2.0}$HAlBEA, $Cu_{2.0}Ni_{2.0}$HAlBEA, $Cu_{4.0}Ni_{2.0}$HAlBEA (results not shown) are very similar and look like typical of BEA structure. It is shown that the crystallinity of BEA zeolite is preserved after introduction of nickel and copper ions in SiBEA and HAlBEA supports. Moreover, as prepared Ni and Cu loaded zeolite samples do not show any evidence of extra-framework compound or amorphization of the zeolite indicating good dispersion of nickel and copper in zeolite structure.

A changes of the position of the narrow main diffraction peak around 2θ of 22.60°, generally taken as evidence of framework contraction–expansion of BEA structure from 22.69° for SiBEA to 22.48° for C-$Cu_{4.0}Ni_{2.0}$SiBEA indicates matrix expansion and incorporation of nickel and copper ions into the framework (Fig. 1).

The introduction of nickel and copper ions into HAlBEA and calcination of such obtained $Cu_{4.0}Ni_{2.0}$HAlBEA involve a small shift of the main diffraction peak from 22.49° for HAlBEA to 22.41° for C-$Cu_{4.0}Ni_{2.0}$HAlBEA suggesting small matrix expansion and incorporation only part of Ni and Cu ions into HAlBEA framework (Fig. 2).

For C-$Cu_{4.0}Ni_{2.0}$SiBEA sample additional phase of CuO is observed suggesting sintering and formation of big crystallites of copper oxide after calcination step. These XRD results are in agreement with the data obtained for low temperature N_2 sorption.

Reduction at 873 K and reaction with 1,2-dichloroethane involve additional changes in C-Cu_xNi_ySiBEA and C-Cu_xNi_yHAlBEA structure as shown by XRD (Figs. 1 and 2).

After reduction of C-$Cu_{4.0}Ni_{2.0}$SiBEA at 873 K CuO reflexes disappeared and in diffractogram of red-C-$Cu_{4.0}Ni_{2.0}$SiBEA (Fig. 1) the reflexes of Cu(0) appear at 2θ of 43.49° and 50.56° and the shift of the main peak of BEA zeolite to higher 2θ value occurs (22.55°). It suggests matrix contraction as a results of output of nickel and copper from framework of BEA zeolite into extra-framework position and formation of Ni(0) and Cu(0) nanoparticles (see chapter 3.5). Such phenomenon was not observed for HAlBEA based catalysts as shown by similar position of the main XRD peak for C-$Cu_{4.0}Ni_{2.0}$HAlBEA and red-C-$Cu_{4.0}Ni_{2.0}$HAlBEA (Fig. 2) suggesting

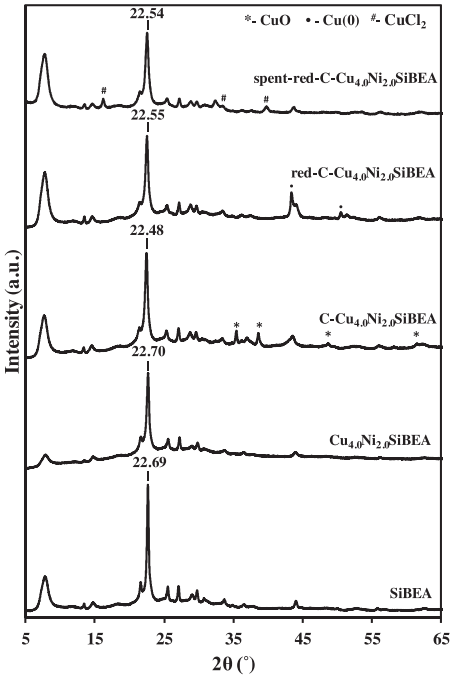

Fig. 1. XRD patterns recorded at ambient atmosphere of SiBEA, $Cu_{4.0}Ni_{2.0}$SiBEA, C-$Cu_{4.0}Ni_{2.0}$SiBEA, red-C-$Cu_{4.0}Ni_{2.0}$SiBEA and spent- red-C-$Cu_{4.0}Ni_{2.0}$SiBEA.

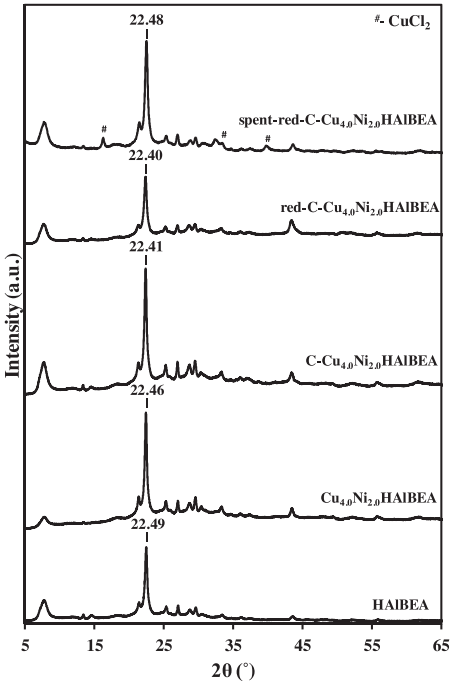

Fig. 2. XRD patterns recorded at ambient atmosphere of HAlBEA, $Cu_{4.0}Ni_{2.0}$HAlBEA, C-$Cu_{4.0}Ni_{2.0}$HAlBEA, red-C-$Cu_{4.0}Ni_{2.0}$HAlBEA and spent-red-C-$Cu_{4.0}Ni_{2.0}$HAlBEA.

that Ni(0) and Cu(0) nanoparticles were formed upon reduction of nickel and copper species present mainly in extra-framework position of C-$Cu_{4.0}Ni_{2.0}$HAlBEA.

The XRD patterns of spent-red-C-$Cu_{4.0}Ni_{2.0}$HAlBEA and spent-red-C-$Cu_{4.0}Ni_{2.0}$SiBEA after reaction of 1,2-dichloroethane are similar to those of red-C-$Cu_{4.0}Ni_{2.0}$HAlBEA and red-C-$Cu_{4.0}Ni_{2.0}$SiBEA but they contain additionally reflexes related to $CuCl_2$ salt (Figs. 1 and 2). It indicates agglomeration of copper chlorine in both catalysts which could lead to deactivation of these catalysts over kinetic run. Moreover, the shift of the position of the main

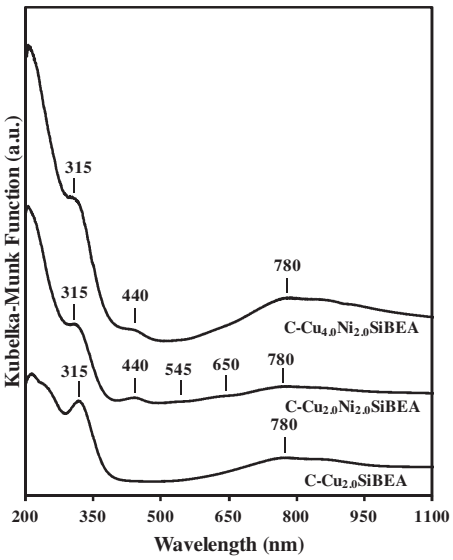

Fig. 3. DR UV–vis spectra recorded at ambient atmosphere of C-$Cu_{2.0}$SiBEA, C-$Cu_{2.0}Ni_{2.0}$SiBEA and C-$Cu_{4.0}Ni_{2.0}$SiBEA.

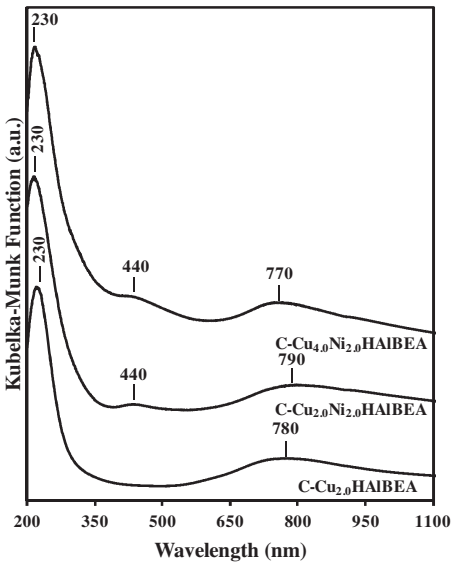

Fig. 4. DR UV–vis spectra recorded at ambient atmosphere of C-$Cu_{2.0}$HAlBEA, C-$Cu_{2.0}Ni_{2.0}$HAlBEA and C-$Cu_{4.0}Ni_{2.0}$HAlBEA.

peak from 2θ of 22.40° for red-C-$Cu_{4.0}Ni_{2.0}$HAlBEA to 22.48° for spent-red-C-$Cu_{4.0}Ni_{2.0}$HAlBEA is probably a results of formation of carbonaceous species, as it has been postulated earlier for zeolite materials [14,15].

3.2. Nature of copper and nickel in Cu_xNi_ySiBEA and Cu_xNi_yHAlBEA from DR UV-vis spectroscopy

Fig. 3 shows, as an example, the DR UV–vis spectra of C-$Cu_{2.0}$SiBEA, C-$Cu_{2.0}Ni_{2.0}$SiBEA and C-$Cu_{4.0}Ni_{2.0}$SiBEA. The spectrum of C-$Cu_{2.0}$SiBEA is composed of a broad band at around 780 nm attributed to d–d transition of Cu(II) ($3d^9$) and the band at around 315 nm probably related to oxygen-to-copper(II) charge transfer (CT) transitions involving framework oxygen and copper present in the zeolite structure as isolated pseudo-tetrahedral Cu(II), in line with earlier reports [17,18]. The absence of UV–vis bands in the range 350–600 nm related to oxygen-to-octahedral copper(II) CT transitions and/or d–d transition of octahedral Cu(II) ($3d^9$) indicates that such copper species are probably not present in C-$Cu_{2.0}$SiBEA, in line with earlier works [19–21].

In the spectrum of bimetallic C-$Cu_{2.0}Ni_{2.0}$SiBEA additional bands at 545 and 650 nm appear related to isolated pseudo-tetrahedral Ni(II) species in line with our recent work on NiSiBEA zeolite [16,22]. However, presence of another band at 440 nm possibly related to octahedral Ni(II) or assigned to oxygen-to-octahedral copper(II) CT transitions and/or d–d transitions of polynuclear Cu(II), suggests the formation of extra-framework Ni(II) and/or Cu(II) species.

For C-$Cu_{4.0}Ni_{2.0}$SiBEA the bands characteristic of isolated pseudo-tetrahedral Ni(II) species are not seen probably due to high concentration of copper. However, at 440 nm intense band attributed to oxygen-to-octahedral copper(II) CT transitions of polynuclear Cu(II) [23,24] is observed indicating probable presence of copper oxide crystallites. These DR UV–vis results are in line with the XRD results presented in Chapter 3.1.

The spectrum of C-$Cu_{2.0}$HAlBEA prepared by conventional wet impregnation method is typical of Cu ion exchanged zeolites with absorption bands at 230 and 780 nm attributed to ligand to metal charge transfer transition and d–d transition of Cu(II) ($3d^9$), respectively. Absorption bands at around 400–600 nm characteristic of CuO and/or Cu_2O are not observed in C-$Cu_{2.0}$HAlBEA (Fig. 4).

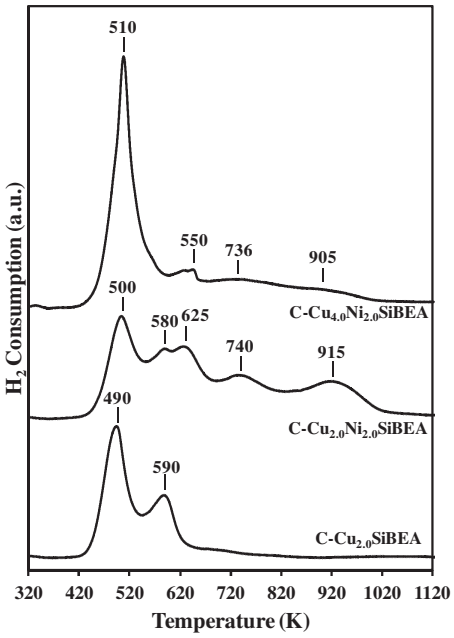

Fig. 5. TPR patterns of C-$Cu_{2.0}$SiBEA, C-$Cu_{2.0}Ni_{2.0}$SiBEA and C-$Cu_{4.0}Ni_{2.0}$SiBEA.

In contrast, in the DR UV–vis spectra of C-$Cu_{2.0}Ni_{2.0}$HAlBEA and C-$Cu_{4.0}Ni_{2.0}$HAlBEA two broad bands at around 440 and 770–790 nm are present (Fig. 4). They are characteristic of both octahedral Ni(II) and Cu(II) extra-framework polynuclear species.

3.3. Reducibility of nickel and copper in C-Cu_xNi_ySiBEA and C-Cu_xNi_yHAlBEA obtained from TPR of H_2

Temperature-programmed reduction experiments were carried out to investigate the reducibility of copper and nickel species present in C-$Cu_{2.0}$SiBEA, C-$Cu_{2.0}Ni_{2.0}$SiBEA and C-$Cu_{4.0}Ni_{2.0}$SiBEA (Fig. 5) and C-$Cu_{2.0}$HAlBEA, C-$Cu_{2.0}Ni_{2.0}$HAlBEA and C-$Cu_{4.0}Ni_{2.0}$HAlBEA (Fig. 6).

TPR pattern of $Cu_{2.0}$SiBEA (Fig. 5) exhibits two symmetric peaks at 490 and 590 K. These peaks are probably due to the reduction of isolated pseudo-tetrahedral copper(II) in two steps, Cu(II) → Cu(I)

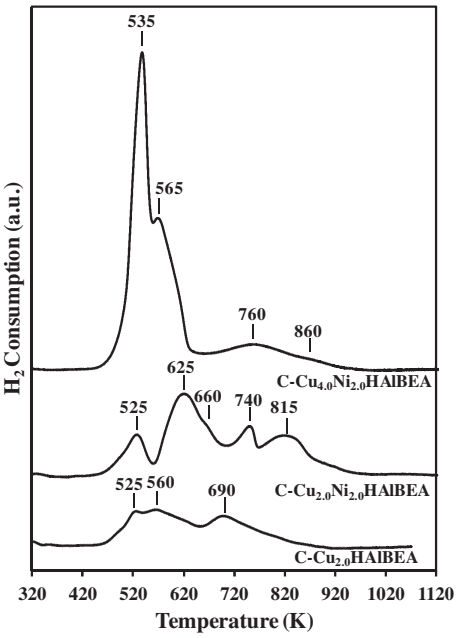

Fig. 6. TPR patterns of C-$Cu_{2.0}$HAlBEA, C-$Cu_{2.0}Ni_{2.0}$HAlBEA and C-$Cu_{4.0}Ni_{2.0}$HAlBEA.

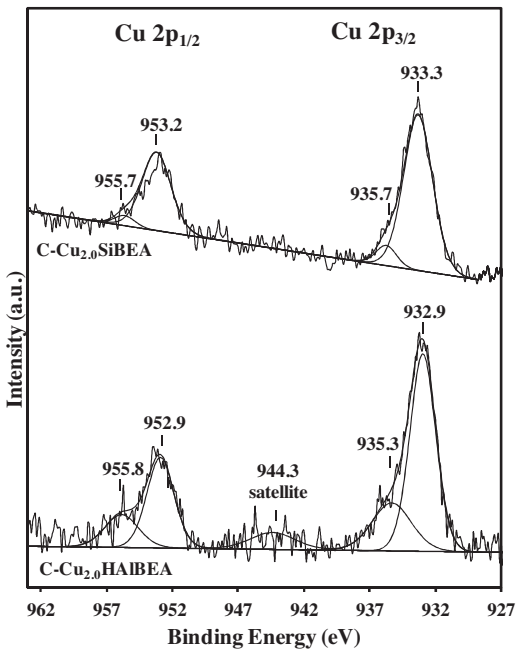

Fig. 7. XP spectra recorded at room temperature of Cu 2p core level of C-$Cu_{2.0}$HAlBEA samples and C-$Cu_{2.0}$SiBEA.

and Cu(I) → Cu(0), respectively, in line with earlier observations by TPR on CuSiBEA zeolites [25]. The first TPR low-temperature peak indicates high reducibility of Cu(II) species, however lower integral area of peak at 590 K may suggest stabilization of Cu(I) species in SiBEA support.

For C-$Cu_{2.0}Ni_{2.0}$SiBEA five reduction peaks with maximum at 500, 580, 625, 740 and 915 K are observed. Two first of them correspond to reduction of copper species because they appear at almost the same temperature as for C-$Cu_{2.0}$SiBEA. The last three signal are most probably related to reduction of nickel(II) species occurring in different environments. As we described recently [16], the observed peaks at 625 K may be attributed to the reduction of octahedral nickel(II) species present in extra-framework position and peaks at 740 and 915 K may be assigned to reduction of two types of pseudo-tetrahedral Ni(II) species strongly interacting with zeolite support.

The presence of well-defined and separated peaks in TPR pattern of C-$Cu_{2.0}Ni_{2.0}$SiBEA corresponding to reduction of copper and nickel species indicates that both Ni(0) and Cu(0) nanoparticles are formed upon 10% H_2/Ar treatment.

In TPR pattern of C-$Cu_{4.0}Ni_{2.0}$SiBEA very intense peak at 510 K appears typical for zeolites containing high amount of copper and/or copper supported oxides [11,12,26,27]. It may be attributed to direct reduction of octahedral copper(II) and/or polynuclear Cu(II) into Cu(0). This result confirms the presence of the copper oxide in C-$Cu_{4.0}Ni_{2.0}$SiBEA in agreement with XRD, low temperature N_2 sorption and DR UV–vis investigations (see the previous chapter).

The TPR pattern of C-$Cu_{2.0}$HAlBEA (Fig. 6) contains three peaks present at 525, 560 and 690 K. The first peak could be attributed to copper cluster and/or copper polynuclear species reduced in one step Cu(II) → Cu(0). Two last peaks may be ascribed to reduction of copper ions at exchange position in two steps, Cu(II) → Cu(I) and Cu(I) → Cu(0), respectively, in line with earlier observations by TPR on Cu-Y [28], Cu-ZSM-5 [29] and Cu-MOR [30] zeolites. However, because of quite broad character of reduction peaks possibility of coexistence of more various Cu(II) species in C-$Cu_{2.0}$HAlBEA cannot be excluded in line with other work on CuBEA zeolite [31].

The pattern of C-$Cu_{2.0}Ni_{2.0}$HAlBEA zeolite shows five peaks (Fig. 6). The first peak could be attributed to copper cluster and/or copper polynuclear species reduced in one step Cu(II) → Cu(0). The peaks at 625 and 660 K may be ascribed to reduction of copper ions at exchange position in two steps, Cu(II) → Cu(I) and Cu(I) → Cu(0), respectively, like for C-$Cu_{2.0}$HAlBEA sample. The signals at 740 and 815 K appear at very similar positions as for nickel containing C-$Ni_{2.0}$HAlBEA described in our earlier work [16,32]. Those peaks were attributed to two different Ni(II) species, probably, to extra-framework octahedral Ni(II) and pseudo-tetrahedral Ni(II) strongly interacting with zeolite structure.

A very intense peak at 535 K (Fig. 6), observed during TPR of C-$Cu_{4.0}Ni_{2.0}$SiBEA, appears typical for zeolites containing high amount of copper and copper supported oxides [11,12,26,27]. It may be attributed to direct reduction of copper cluster and/or copper polynuclear species reduced in one step Cu(II) → Cu(0) in C-$Cu_{4.0}Ni_{2.0}$HAlBEA.

3.4. Chemical nature and environment of nickel and copper in C-Cu_xNi_ySiBEA and C-Cu_xNi_yHAlBEA obtained by XPS

To describe the chemical nature and environment of copper in C-$Cu_{2.0}$SiBEA and C-$Cu_{2.0}$HAlBEA (Fig. 7) and copper and nickel in C-$Cu_{2.0}Ni_{2.0}$SiBEA and C-$Cu_{2.0}Ni_{2.0}$HAlBEA (Figs. 8 and 9), respectively, the photoelectron spectroscopy was used. The XPS experiments were carried out in the BE region correspond to Cu 2p, Ni 2p, Si 2p, O 1s, Al 2p, and C 1s core excitations.

The Si 2p BE values of ~103.4–104 eV for C-$Cu_{2.0}$HAlBEA, C-$Cu_{2.0}Ni_{2.0}$HAlBEA C-$Cu_{2.0}$SiBEA and C-$Cu_{2.0}Ni_{2.0}$SiBEA samples are close to that observed for other zeolites containing Cu and Ni [33]. The O 1s XP spectra contain main peak at 533.0–533.4 eV, which can be attributed to oxygen in Si—O—Si or Si—O—Al environment in line earlier work on zeolites [34,35]. The BE values of Al 2p for no dealuminated samples are typical of zeolite with high Si/Al ratio like ZSM-5 [35].

XP spectra of C-$Cu_{2.0}$SiBEA and C-$Cu_{2.0}$HAlBEA (Fig. 7) in the range of binding energy of Cu 2p contain two doublets at 933–937 and 953–957 eV characteristic of Cu(II) [36,37]. The most intensive peaks of Cu $2p_{3/2}$ at about 933 eV and of Cu $2p_{1/2}$ at about of 953 eV are probably related to well dispersed pseudo-tetrahedral Cu(II)

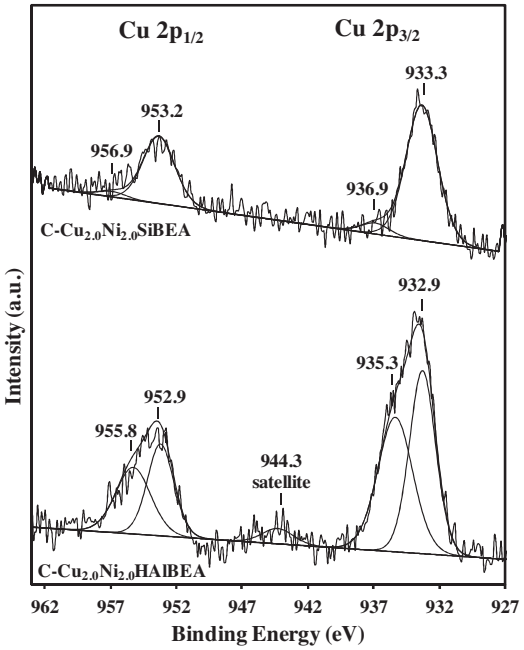

Fig. 8. XP spectra recorded at room temperature of Cu 2p core level of C-$Cu_{2.0}Ni_{2.0}$HAlBEA and C-$Cu_{2.0}Ni_{2.0}$SiBEA.

species. In contrast, the peaks of Cu $2p_{3/2}$ at about 935 eV and of Cu $2p_{1/2}$ at about 956 eV present in the spectra of C-$Cu_{2.0}$SiBEA and C-$Cu_{2.0}$HAlBEA may be attributed to copper(II) species in octahedral coordination, in line with earlier reports on CuBEA zeolites [25,33].

Additionally, absence of satellite peak in the XP spectrum of C-$Cu_{2.0}$SiBEA is probably due to very high dispersion and incorporation of copper ions into zeolite matrix.

For C-$Cu_{2.0}Ni_{2.0}$SiBEA the XP spectrum in Cu 2p region is very similar to the spectrum of C-$Cu_{2.0}$SiBEA and reveals two signals of Cu $2p_{3/2}$, first main signal at 933.3 eV attributed to Cu(II) species, the most probably to isolated pseudo-tetrahedral Cu(II) and

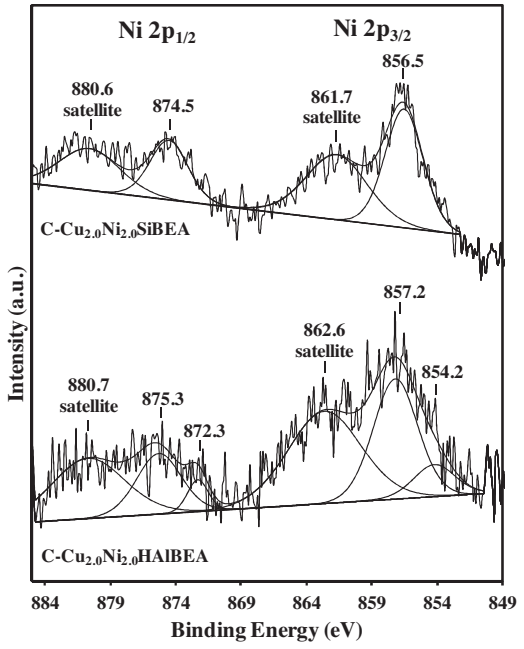

Fig. 9. XP spectra recorded at room temperature of Ni 2p core level of C-$Cu_{2.0}Ni_{2.0}$HAlBEA and C-$Cu_{2.0}Ni_{2.0}$SiBEA.

second small one at 936.9 eV suggesting presence of a little amount of octahedral Cu(II) species (Fig. 8).

As shown in Fig. 8, for C-$Cu_{2.0}Ni_{2.0}$HAlBEA the XP spectrum exhibits two peaks of Cu $2p_{3/2}$. The peak at BE value of 932.9 eV may be attributed to pseudo-tetrahedral Cu(II), being in strong interaction with the zeolite framework. On the other hand, the peak at 935.3 eV may be attributed to Cu(II) in octahedral coordination. Moreover, higher intensity of second peaks suggests higher concentration of octahedral Cu(II) species in C-$Cu_{2.0}Ni_{2.0}$HAlBEA than in C-$Cu_{2.0}Ni_{2.0}$SiBEA zeolite.

In the XPS spectrum of C-$Cu_{2.0}Ni_{2.0}$SiBEA (Fig. 9) in the region of Ni 2p two bands at about 856 and 874 eV are observed characteristic of well dispersed pseudo-tetrahedral Ni(II) [36–39].

On the other hand, in the XPS spectrum of C-$Cu_{2.0}Ni_{2.0}$HAlBEA in the range of Ni 2p there are four peaks. Two main at 857.2 and 875.3 eV which may be assigned to pseudo-tetrahedral Ni(II) and two minor ones at 854.2 and 872.2 eV attributed to octahedral Ni(II) in line with earlier report [40,41].

These XPS results confirm that nickel and copper in C-$Cu_{2.0}Ni_{2.0}$SiBEA is mainly present as mononuclear pseudo-tetrahedral Ni(II) and Cu(II) species incorporated into framework of zeolite. However, in case of C-$Cu_{2.0}Ni_{2.0}$HAlBEA copper and nickel occur as a mixture of tetrahedral and octahedral species.

3.5. Size and distribution of Cu and Ni nanoparticles in red-C-$Cu_{2.0}Ni_{2.0}$HAlBEA and red-C-$Cu_{2.0}Ni_{2.0}$SiBEA obtained by TEM

The way of catalysts preparation has a great impact of metal particle distribution and particle diameter. The catalysts prepared by two-steps postsynthesis procedure and reduced in flowing mixture of H_2/Ar contain very well dispersed nanoparticles. The size of Cu(0) nanoparticles in red-C-$Cu_{2.0}$SiBEA (Fig. 10) is in the range of 1–5 nm, however more than 86% of nanoparticles have the size lower than 3 nm. Similar results was observed for red-C-$Cu_{2.0}Ni_{2.0}$SiBEA where in addition nanoparticles with diameter of 1 nm appear, probably as isolated Ni(0) nanoparticles, in line with earlier reports on nickel containing zeolites [22,29].

In the case of analogous red-C-$Cu_{2.0}$HAlBEA and red-C-$Cu_{2.0}Ni_{2.0}$HAlBEA (Fig. 11), prepared by conventional wet impregnation, the nanoparticles are much larger and their sizes are in the range of 2–14 and 2–11 nm, respectively. However, the much worse distribution of nanoparticles size is observed in red-C-$Cu_{4.0}Ni_{2.0}$SiBEA and red-C-$Cu_{4.0}Ni_{2.0}$HAlBEA with higher Cu content due to the formation in their structure of extra-framework polynuclear and/or copper oxide.

Furthermore, the more detailed investigations of red-C-$Cu_{2.0}Ni_{2.0}$SiBEA and red-C-$Cu_{2.0}Ni_{2.0}$HAlBEA performed by HRTEM allows determining significant differences between both catalysts prepared by two different methods. In red-C-Cu_xNi_yHAlBEA catalysts nickel and copper nanoparticles are situated very closely (Fig. 12) and for red-C-$Cu_{2.0}Ni_{2.0}$SiBEA copper and nickel nanoparticles exist separately, such as was presented in Fig. 12. This phenomenon probably is related to the method of preparation of both materials and it should be taken in consideration for all of the catalysts in interpretation of their catalytic activity.

The two-step postsynthesis procedure applied for C-Cu_xNi_ySiBEA preparation allows to incorporate copper and nickel ions into framework of BEA as pseudo-tetrahedral Cu(II) and Ni(II). In consequence, after reduction in flowing H_2/Ar at 873 K, in the red-C-Cu_xNi_ySiBEA catalysts a very good dispersion of metallic Cu(0) and Ni(0) nanoparticles was observed with very small size of nanoparticles between 1 and 5 nm (Fig. 10). On the other hand, application of the conventional wet impregnation method leads to formation of much bigger copper and nickel nanoparticles in red-C-Cu_xNi_yHAlBEA catalysts with the size of nanoparticles

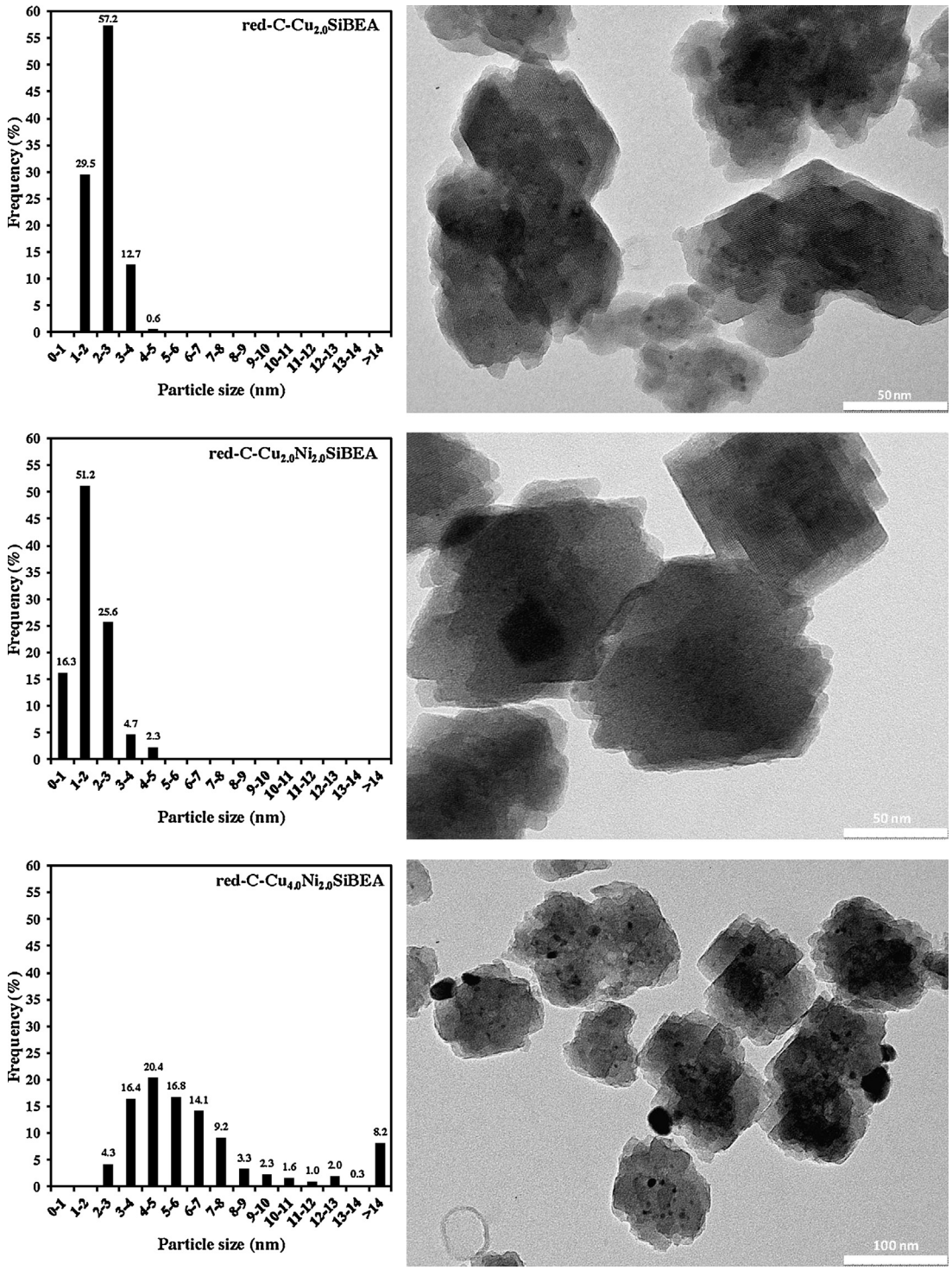

Fig. 10. Histograms of metal particles distribution and TEM images of red-C-$Cu_{2.0}$SiBEA, red-C-$Cu_{2.0}Ni_{2.0}$SiBEA and red-C-$Cu_{4.0}Ni_{2.0}$SiBEA.

between 2 and 12 nm (Fig. 11), bigger than that observed in catalysts prepared by two-step postsynthesis procedure (Fig. 10).

Very interesting informations were obtained from the HRTEM measurement of red- and spent-red-: C-$Cu_{2.0}Ni_{2.0}$SiBEA and C-$Cu_{2.0}Ni_{2.0}$HAlBEA (Figs. 13 and 14). Any changes in nanoparticles size and distribution were observed for spent-red-C-$Cu_{2.0}Ni_{2.0}$SiBEA and only very slight modification in particles diameters in the case of spent-red-C-$Cu_{2.0}Ni_{2.0}$HAlBEA (Figs. 12–14).

Our earlier HRTEM investigations of red-C-$Ni_{2.0}$SiBEA and red-C-$Ni_{2.0}$HAlBEA before and after reaction of 1,2-dichloroethane evidenced slight sintering of nickel particles in the case of spent-red-C-$Ni_{2.0}$SiBEA and much stronger in the case of spent-red-C-$Ni_{2.0}$HAlBEA. It suggests beneficial role of the copper whose presence in both type of catalysts prevents the sintering of metal nanoparticles.

4. Catalytic activity

The results obtained for reaction of 1,2-dichloroethane over red-C-Cu_xNi_ySiBEA and red-C-Cu_xNi_yHAlBEA are shown in Figs. 15–18. Figs. 15 and 16 show changes of conversion as a function of time on stream (TOS) over 2 series of catalysts. It is seen that during

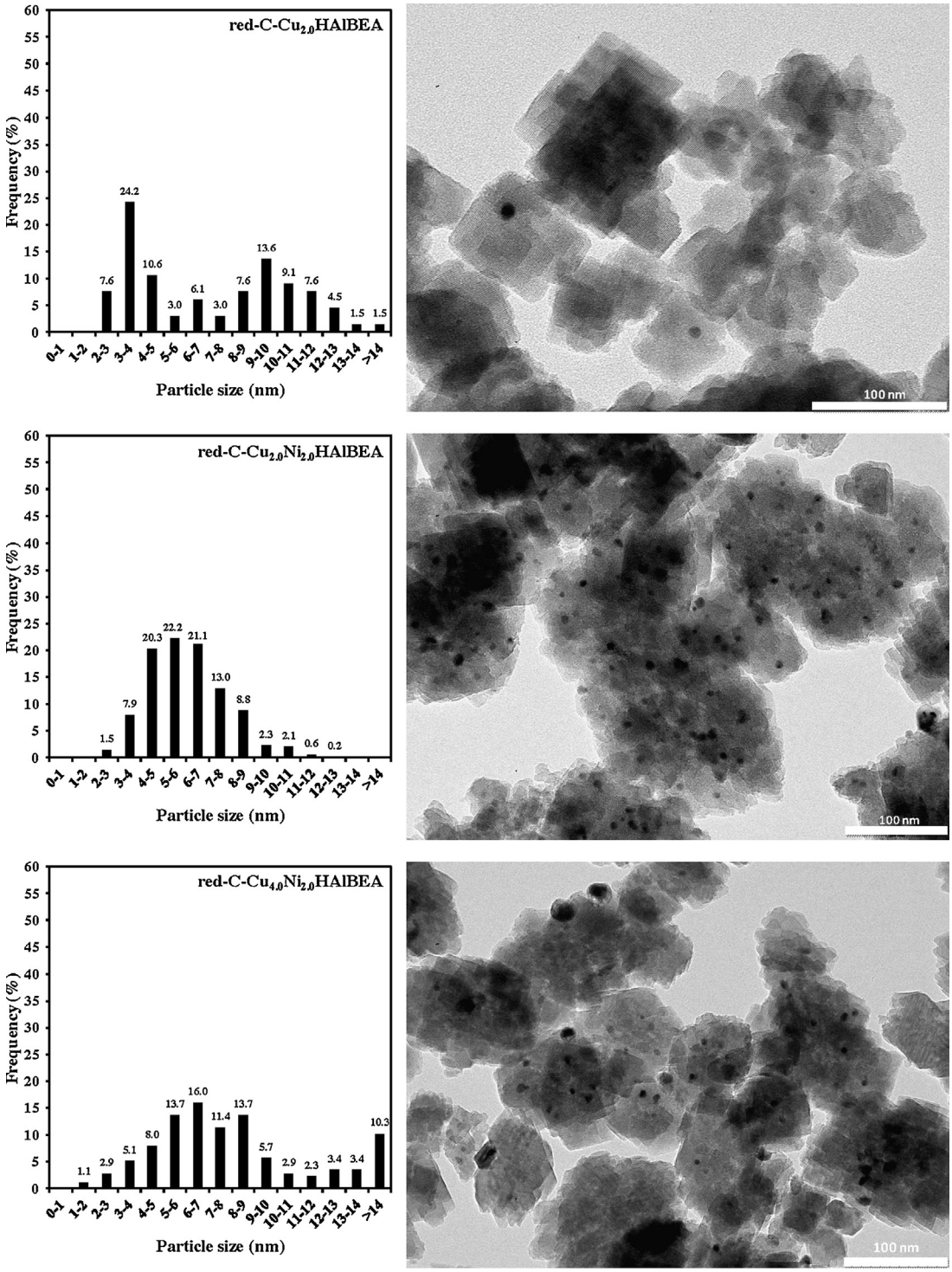

Fig. 11. Histograms of metal particles distribution and TEM images of red-C-$Cu_{2.0}$HAlBEA, red-C-$Cu_{2.0}Ni_{2.0}$HAlBEA and red-C-$Cu_{4.0}Ni_{2.0}$HAlBEA.

~17 h period of screening the overall conversion is very similar for red-C-Cu_xNi_ySiBEA (Fig. 16). For red-C-Cu_xNi_yHAlBEA strong deactivation of catalyst during the reaction is observed (Fig. 16). Activity of catalysts is changed with the composition of the metallic phase and loading of metals (Table 2). For red-C-Cu_xNi_ySiBEA, the lowest value of overall conversion, and the lowest activity was observed for SiBEA support and Cu-containing SiBEA (respectively 0.01 $\mu mol\,s^{-1}\,g_{cat}^{-1}$ for red-C-SiBEA and 0.03 $\mu mol\,s^{-1}\,g_{cat}^{-1}$ for red-C-$Cu_{2.0}$SiBEA), what is in agreement with investigations for typical metals/support systems, where copper was inactive or showed much lower than nickel activity in catalytic conversion of chloroorganic compounds [42,43]. The highest value of conversion and activity per gram of catalyst was observed for monometallic nickel catalyst (0.39 $\mu mol\,s^{-1}\,g_{cat}^{-1}$). Addition of 2 wt.% of nickel to copper leads to increasing of the activity of bimetallic samples. Negligible differences in catalytic behaviour of red-C-$Cu_{2.0}Ni_{2.0}$SiBEA (reaction rate of 0.22 $\mu mol\,s^{-1}\,g_{cat}^{-1}$) and red-C-$Cu_{4.0}Ni_{2.0}$SiBEA (reaction rate of 0.17 $\mu mol\,s^{-1}\,g_{cat}^{-1}$) could suggest a weak interaction between both kind of metals and/or a low amount of copper–nickel alloys present in both catalysts (Table 2).

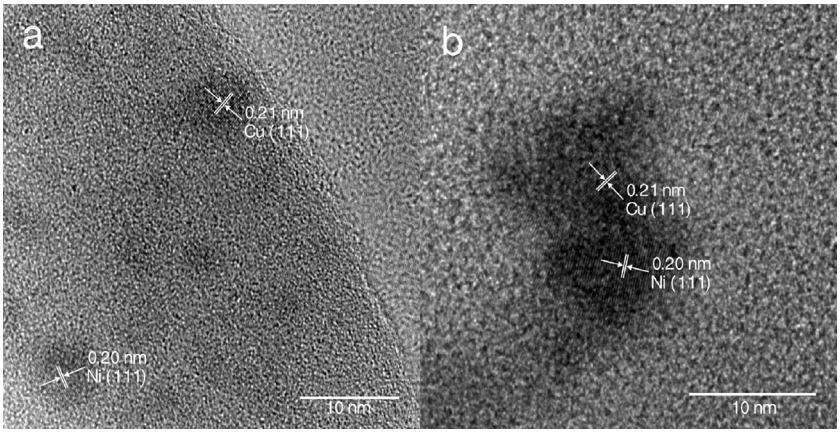

Fig. 12. HRTEM results for red-C-$Cu_{2.0}Ni_{2.0}$SiBEA (a) and red-C-$Cu_{2.0}Ni_{2.0}$HAlBEA (b).

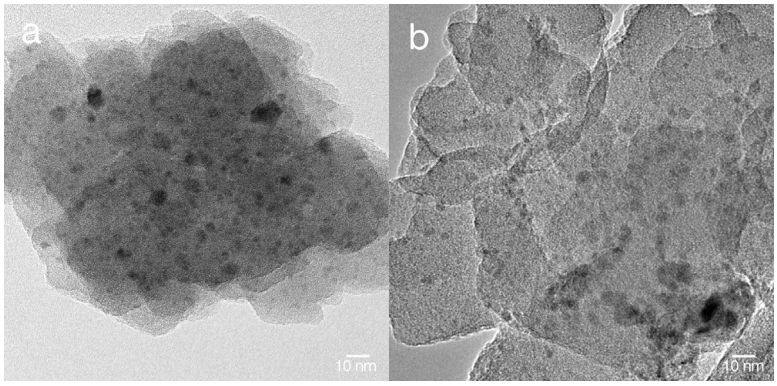

Fig. 13. HRTEM results for red-C-$Cu_{2.0}Ni_{2.0}$SiBEA (a) and spent-red-C-$Cu_{2.0}Ni_{2.0}$SiBEA (b).

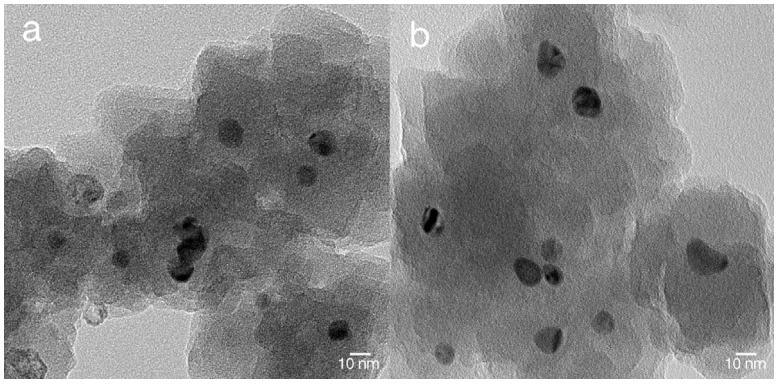

Fig. 14. HRTEM results for red-C-$Cu_{2.0}Ni_{2.0}$HAlBEA (a) and spent-red-C-$Cu_{2.0}Ni_{2.0}$HAlBEA (b).

Table 2
Catalytic conversion of 1,2-dichloroethane over red-C-Cu_xNi_ySiBEA and red-C-Cu_xNi_yHAlBEA. Overall activity and selectivity to the products at temperature range of 523 K at steady state condition.

Catalyst	Activity ($\mu mol\ s^{-1}\ g^{-1}_{cat}$)	Selectivity (%) C_2H_4	C_2H_3Cl	Others[a]
Red-C-SiBEA	0.01	0.62	99.38	–
Red-C-$Cu_{2.0}$SiBEA	0.03	75.59	24.41	–
Red-C-$Cu_{2.0}Ni_{2.0}$SiBEA	0.22	96.40	3.60	–
Red-C-$Cu_{4.0}Ni_{2.0}$SiBEA	0.17	97.96	2.13	–
Red-C-$Ni_{2.0}$SiBEA	0.39	91.87	0.66	7.47
Red-C-HAlBEA	0.33	0.41	99.59	–
Red-C-$Cu_{2.0}$HAlBEA	0.25	1.35	98.65	–
Red-C-$Cu_{2.0}Ni_{2.0}$HAlBEA	0.38	7.84	91.62	0.54
Red-C-$Cu_{4.0}Ni_{2.0}$HAlBEA	0.64	7.77	92.04	0.19
Red-C-$Ni_{2.0}$HAlBEA	0.32	9.52	72.85	17.63

[a] Mainly C_1–C_3 hydrocarbons and chlorohydrocarbons like: C_2H_6, C_3H_6, CH_2Cl_2, C_2H_5Cl, 1,1-$C_2H_2Cl_2$, 1,2-$C_2H_2Cl_2$.

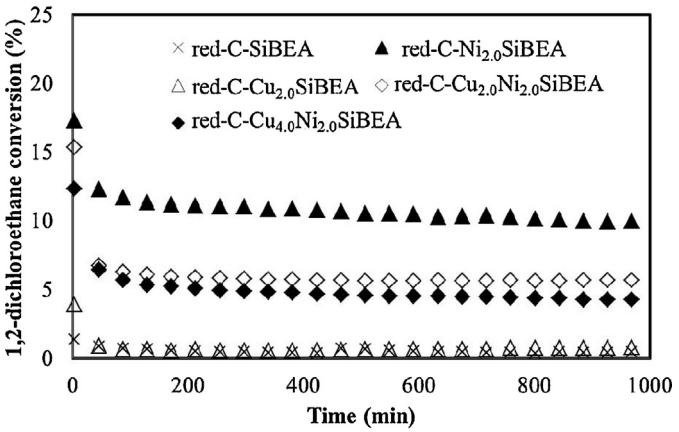

Fig. 15. Time on stream behaviour during hydrodechlorination of 1,2-dichloroethane over red-C-Ni_xCu_ySiBEA at 523 K – overall conversion.

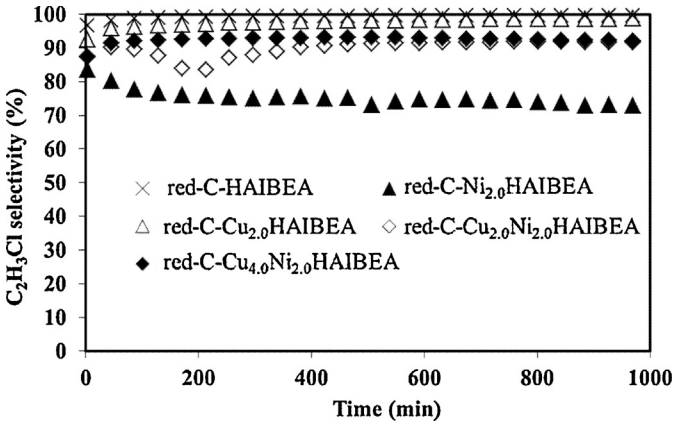

Fig. 18. Time on stream behaviour during dehydrochlorination of 1,2-dichloroethane over red-C-Ni_xCu_yHAlBEA at 523 K – selectivity to vinyl chloride.

Results obtained for red-C-$Cu_{2.0}Ni_{2.0}$SiBEA and red-C-Cu_xNi_yHAlBEA (Table 2) show a big difference between two series of catalysts. Red-C-$Cu_{2.0}$HAlBEA (with reaction rate of 0.25 μmol s^{-1} g_{cat}^{-1}) is active in hydrogen assisted dehydrochlorination of 1,2-dichloroethane into vinyl chloride with conversion of 1,2-dichloroethane of higher than 10% in the large range of temperature and very stable as a function of time. In contrast, red-C-$Cu_{2.0}$SiBEA is not active in this reaction with very small conversion of 1,2-dichloroethane, close to that of SiBEA support (Fig. 15). The high activity of red-C-$Cu_{2.0}$HAlBEA is probably related to high acidity of this catalyst. The higher activity of red-C-HAlBEA support (with reaction rate of 0.33 μmol s^{-1} g_{cat}^{-1}) than that of red-C-$Cu_{2.0}$HAlBEA (with reaction rate of 0.26 μmol s^{-1} g_{cat}^{-1}) with modified acidity confirm this supposition. However, red-C-$Cu_{2.0}$HAlBEA catalyst is more resistant to deactivation than HAlBEA support. It seems that the presence of copper in red-C-$Cu_{2.0}$HAlBEA catalyst plays beneficial role by alteration of the acidic properties of this material. Additionally, thanks to high affinity of Cu(0) to chlorine it could purify active centers of beta zeolite from chlorine containing species.

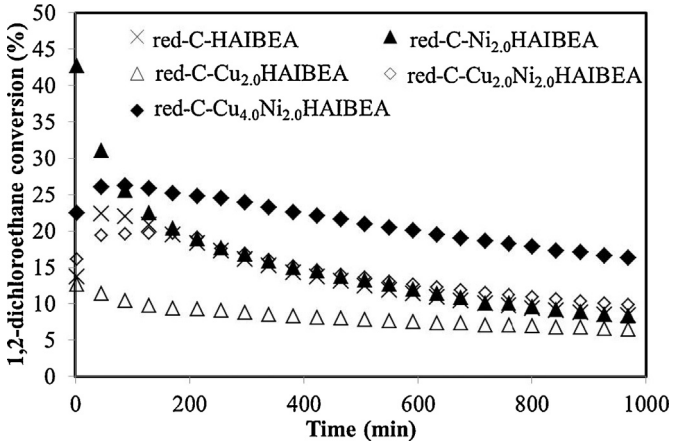

Fig. 16. Time on stream behaviour during dehydrochlorination of 1,2-dichloroethane over red-C-Cu_xNi_yHAlBEA at 523 K – overall conversion.

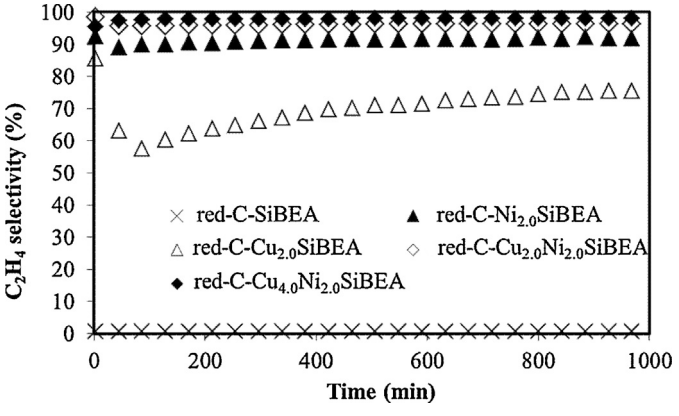

Fig. 17. Time on stream behaviour during hydrodechlorination of 1,2-dichloroethane over red-C-Ni_xCu_ySiBEA at 523 K – selectivity to ethylene.

The highest overall conversion (Fig. 16) and the highest reaction rate (0.64 μmol s^{-1} g_{cat}^{-1}) are achieved for red-C-$Cu_{4.0}Ni_{2.0}$HAlBEA system (Table 2). This specific synergistic effect can be related to very good alloying of copper–nickel species in this system.

Moreover, an important impact on catalytic behaviour of red-C-$Cu_{4.0}Ni_{2.0}$HAlBEA could be related to the presence of metal particles bigger than 15 nm. It was reported that in some cases the big nanoparticles of metals can strongly resist to deactivation by adsorption of hydrochloride than the smaller nanoparticles [44,45]. The time on stream behaviour obtained for red-C-$Cu_{2.0}Ni_{2.0}$HAlBEA catalyst have shown slightly higher activity of this system than in case red-C-HAlBEA support and red-C-$Ni_{2.0}$HAlBEA catalyst, and it confirms beneficial role of coexistence of Cu(0) and Ni(0) nanoparticles and presence of small amount of Cu–Ni alloy.

Very important information could be obtained by analyzing the results of selectivity toward the products of catalytic conversion of 1,2-dichloroethane. The main product of hydrodechlorination on red-C-Cu_xNi_ySiBEA is ethylene (Fig. 17). Approximately 100% of the selectivity to this desired product was achieved for these bimetallic systems (Table 2). This indicates that the presence of very small, separated and well dispersed Ni(0) and Cu(0) nanoparticles improve the selectivity toward ethylene. Increasing selectivity to unsaturated hydrocarbons during hydrodechlorination of chlorinated alkanes is typical for noble metal modified by copper or silver catalysts [8,43,46,47]. The literature dealing with hydrodechlorination application of modified nickel catalysts, especially with copper doped nickel catalysts is rather scarce. The application of such catalysts results in formation of chloroorganic products such as vinyl chloride during HdCl of 1,1,2-trichloroethane [42] or hydrogen-assisted dechlorination of 1,2-dichloroethane [48]. So, the catalysts prepared by two-step post-synthesis procedure behave rather like copper–noble metal systems [8,43] or monometallic nickel catalysts [22,49].

Another situation is observed for red-C-Cu_xNi_yHAlBEA catalysts (Fig. 18). The main product of 1,2-dichloroethane conversion on these systems is vinyl chloride and this is in agreement with the results obtained for analogous catalysts in hydrogen-assisted dechlorination [48]. The highest selectivity (~100%) toward this product is obtained for red-C-HAlBEA support (Fig. 18). In contrast, the introduction of copper in red-C-HAlBEA support involve to a little decreasing of selectivity to vinyl chloride as shown for red-C-$Cu_{2.0}$HAlBEA in Fig. 18.

Although, the reaction conditions have been still the same, dependently of the kind of materials used as catalysts the role of hydrogen in reaction was completely different. During hydrodechlorination of 1,2-dichloroethane over red-C-Cu_xNi_ySiBEA, the presence of hydrogen is essential for ethylene formation. Whereas, the dehydrochlorination over red-C-Cu_xNi_yHAlBEA is associated with the presence mainly Brønsted acidic sites responsible for transformation of 1,2-dichloroethane towards vinyl chloride. So, the presence of hydrogen in reaction mixture may play the role in reconstruction and regeneration of acidic active centers, and leads to the formation of small amounts of olefins like ethylene and propene (Table 2.).

4.1. Temperature-programmed hydrogenation (TPH) of spent catalysts

Interesting information follows from the temperature-programmed hydrogenation of deposit retained by the Cu–Ni catalysts after conversion of 1,2-dichloroethane (results not shown). During this reaction on red-C-Cu_xNi_yHAlBEA and red-C-Cu_xNi_ySiBEA catalysts both carbon and chlorine species are formed, in line with extensive investigation of Heinrichs et al. [50] for bimetallic Pd–Ag catalysts. The catalysts prepared by two-step post-synthesis procedure contain much less carbon and chlorine than the materials prepared by conventional wet impregnation.

5. Conclusions

The physiochemical characterization experiments carried out in this work have shown that two-step postsynthesis procedure applied for preparation of red-C-Cu_xNi_ySiBEA is an effective way to obtain catalysts with separated and well dispersed Cu(0) and Ni(0) nanoparticles.

Red-C-$Cu_{2.0}Ni_{2.0}$SiBEA and red-C-$Cu_{4.0}Ni_{2.0}$SiBEA are excellent catalysts for complete hydrodechlorination of 1,2-dichloroethane to ethylene, desired product of this reaction.

HRTEM and TPH results obtained for spent-red-C-$Cu_{2.0}Ni_{2.0}$SiBEA catalyst reveal no metal particles sintering in this catalyst and low poisoning with chloride and carbonaceous deposit.

Red-C-Cu_xNi_yHAlBEA catalysts prepared by conventional wet impregnation method are characterized by formation of much bigger metal particles and non-homogeneity of Ni(0) and Cu(0) nanoparticles. However, for these catalysts very high selectivity into vinyl chloride (~100%) is observed, second desired product of catalytic conversion of 1,2-dichloroethane.

Acknowledgments

The POMOST/2011-4/11 project is realized within the “Parent Bridge Programme” of Foundation for Polish Science, cofinanced from European Union, Regional Development Fund (AŚ, SD). Special thanks are due to C. Calers (Laboratoire de Reactivite de Surface,Paris) for performing the XPS measurements.

References

[1] E. Goldberg, Sci. Total Environ. 100 (1991) 17–28.
[2] V.I. Simagina, O.V. Netskina, E.S. Tayban, O.V. Komova, E.D. Grayfer, A.V. Ischenko, E.M. Pazhetnov, Appl. Catal. A 379 (2010) 87–94.
[3] N. Seshu Babu, N. Lingaiah, P.S. Sai Prasad, Appl. Catal. B 111–112 (2012) 309–316.
[4] H.-L. Lien, W.-X. Zhang, Appl. Catal. B 77 (2007) 110–116.
[5] T. Zhoua, Y. Li, T.-T. Lima, Sep. Purif. Technol. 76 (2010) 206–214.
[6] B. Yang, S. Deng, G. Yu, Y. Lu, H. Zhang, J. Xiao, G. Chen, X. Cheng, L. Shi, Chem. Eng. J. 219 (2013) 492–498.
[7] B. Yang, S. Deng, G. Yu, H. Zhang, J. Wu, Q. Zhuo, J. Hazard. Mater. 189 (2011) 76–83.
[8] S. Lambert, F. Ferauche, A. Brasseur, J.-P. Pirard, B. Heinrichs, Catal. Today 100 (2005) 283–289.
[9] H. Chen, S. Wang, M. Xiao, D. Han, Y. Lu, Y. Meng, Chin. J. Chem. Eng. 20 (2012) 906–913.
[10] F. Habimana, X. Li, S. Ji, B. Lang, D. Sun, C. Li, J. Nat. Gas Chem. 18 (2009) 392–398.
[11] A.C. Furtado, C. Goncalves Alonso, M. Pereira Cantao, N.R. Camargo Fernandes-Machado, Int. J. Hydrogen Energy 36 (2011) 9653–9662.
[12] J. Alvarez-Rodriguez, M. Cerro-Alarcon, A. Guerrero-Ruiz, I. Rodriguez-Ramos, A. Arcoya, Appl. Catal. A 348 (2008) 241–250.
[13] H. Noller, W.N. Lin, J. Catal. 85 (1984) 25–30.
[14] I. Hannus, Appl. Catal. A 189 (1999) 263–276.
[15] A.S. Shalygin, L.V. Malyshheva, E.A. Paukshtis, Kinet. Catal. 52 (2011) 305–315.
[16] A. Śrębowata, R. Baran, D. Łomot, D. Lisovytskiy, T. Onfroy, S. Dzwigaj, Appl. Catal. B 147 (2014) 208–220.
[17] G. Moretti, C. Dossi, A. Fusi, S. Recchia, R. Psaro, Appl. Catal. B 20 (1999) 67–73.
[18] M.H. Groothaert, J.A. Van Bokhoven, A.A. Battiston, B.M. Weckhuysen, R.A. Schoonheydt, J. Am. Chem. Soc. 125 (2003) 7629–7640.
[19] M.H. Groothaert, P.J. Smeets, B.F. Sels, P.A. Jacobs, R.A. Schoonheydt, J. Am. Chem. Soc. 127 (2005) 1394–1395.
[20] H. Praliaud, S. Mikhailenko, Z. Chajar, M. Primet, Appl. Catal. B 16 (1998) 359–374.
[21] R.A. Schoonheydt, Catal. Rev. Sci. Eng. 35 (1993) 129–168.
[22] R. Baran, I.I. Kamińska, A. Śrębowata, S. Dzwigaj, Micropor. Mesopor. Mat. 169 (2013) 120–127.
[23] K.I. Shimizu, R. Maruyama, T. Hatamachi, T. Kodama, J. Phys. Chem. C 111 (2007) 6440–6446.
[24] E.I. Solomon, P. Chen, M. Metz, S. Lee, A.E. Palmer, Angew. Chem. Int. Ed. 40 (2001) 4570–4590.
[25] S. Dzwigaj, J. Janas, J. Mizera, J. Gurgul, R.P. Socha, M. Che, Catal. Lett. 126 (2008) 36–42.
[26] D.L. Hoang, T.T.H. Dang, J. Engeldinger, M. Schneider, J. Radnik, M. Richter, A.J. Martin, Solid State Chem. 184 (2011) 1915–1923.
[27] J. Ashok, M. Subrahmanyam, A. Venugopal, Int. J. Hydrogen Energy 33 (2008) 2704–2713.
[28] M. Richter, M.J.G. Fait, R. Eckelt, E. Schreier, M. Schneider, M.-M. Pohl, R. Fricke, Appl. Catal. B 73 (2007) 269–281.
[29] M.J. Jia, W.X. Zhang, T.H. Wu, J. Mol. Catal. A 185 (2002) 151–157.
[30] C. Torre-Abreu, C. Henriques, F.R. Ribeiro, G. Delahay, M.F. Ribeiro, Catal. Today 54 (1999) 407–418.
[31] R. Kefirov, A. Penkova, K. Hadjiivanov, S. Dzwigaj, M. Che, Micropor. Mesopor. Mat. 116 (2008) 180–187.
[32] R. Baran, A. Śrębowata, I.I. Kamińska, D. Łomot, S. Dzwigaj, Micropor. Mesopor. Mat. 180 (2013) 209–218.
[33] J. Janas, J. Gurgul, R.P. Socha, S. Dzwigaj, Appl. Catal. B 91 (2009) 217–224.
[34] M. Stocker, Microporous Mater. 6 (1996) 235–257.
[35] W. Grunert, R. Schlogl, Mol. Sieves 4 (2004) 467–515.
[36] N. Liu, R. Zhang, B. Chen, Y. Li, Y. Li, J. Catal. 294 (2012) 99–112.
[37] A. Corma, A. Palomares, F. Marquez, J. Catal. 170 (1997) 132–139.
[38] S. Bendezu, R. Cida, J.L.G. Fierro, A. López Agudo, Appl. Catal. A 197 (2000) 47–60.
[39] H. Kim, K. Kang, H. Kwak, J.H. Kim, Chem. Eng. J. 168 (2011) 775–783.
[40] Y. Matsumura, K. Tanaka, N. Tode, T. Yazawa, M. Haruta, J. Mol. Catal. A 152 (2000) 157–165.
[41] T. Lehmann, T. Wolff, C. Hamel, P. Veit, B. Garke, A. Seidel-Morgenstern, Micropor. Mesopor. Mat. 151 (2012) 113–117.
[42] Y.H. Choi, W.Y. Lee, J. Mol. Catal. A 174 (2001) 193–204.
[43] A. Śrębowata, W. Lisowski, J.W. Sobczak, Z. Karpiński, Catal. Today 175 (2011) 576–584.
[44] R. Gopinath, K.N. Rao, P.S.S. Prasad, S.S. Medhavendra, S. Narayanan, G. Vivekanandan, J. Mol. Catal. A 181 (2002) 215–220.
[45] M. Bonarowska, Z. Kaszkur, L. Kepiński, Z. Karpiński, Appl. Catal. B 99 (2010) 248–256.
[46] Y. Han, J. Zhou, W. Wang, H. Wan, Z. Xu, S. Zheng, D. Zhu, Appl. Catal. B 125 (2012) 172–179.
[47] X. Wei, A.-Q. Wang, X.-F. Yang, L. Li, T. Zhang, Appl. Catal. B 121–122 (2012) 105–114.
[48] W. Juszczyk, J.C. Colmenares, A. Śrębowata, Z. Karpiński, Catal. Today 169 (2011) 186–191.
[49] A. Śrębowata, W. Juszczyk, Z. Kaszkur, J.W. Sobczak, L. Kępiński, Z. Karpiński, Appl. Catal. A 319 (2007) 181–192.
[50] B. Heinrichs, F. Noville, J.-P. Schoebrechts, J.-P. Pirard, J. Catal. 220 (2003) 215–225.